



# Experimental Investigation on Microstructure and Mechanical Properties of Laser-Welded Nb-1% Zr-0.1% C Alloy

Santosh Kumar Gupta , Sanjib Jaypuria, Dilip Kumar Pratihari, and Partha Saha

Submitted: 17 November 2020 / Revised: 18 May 2021 / Accepted: 8 June 2021 / Published online: 22 June 2021

Nb-1%Zr-0.1%C alloy is mostly used in high-temperature reactor (HTR) as a structural material, due to its high-temperature strength, resistance to irradiation and nuclear environment. In the present study, the issues related to control and optimization of laser welding parameters are dealt in order to obtain the welded joints with satisfactory strength and ductility. Laser butt welding of 0.5 mm thin sheets is conducted in continuous wave mode to analyze the significance and influence of process parameters, i.e., beam diameter, welding speed and laser power on the mechanical and metallurgical properties of the joints. Welding speed is found to be the most significant process parameter, which controls the changes in the mechanical and metallurgical properties. Bead profile, hardness, tensile strength, microstructural and phase variations in these joints are evaluated to study their dependence on the welding speed varied in the three levels of 1000 mm/min, 1250 mm/min and 1500 mm/min. Welding speed alters the cooling rate; cooling rate regulates the grain refinement, phase change and ultimately alters the hardness, and tensile strength of the fusion zone (FZ). The increment in hardness value in the FZ and loss of ductility as compared to base metal can be attributed to some hard and brittle phases ( $Nb_6C_5$  and NbC) formed due to increased welding speed. The failure of the welded joints after the tension tests is observed to be located in both FZ and the base metal, that indicates both the brittle and ductile modes of failure in the FZ of the samples having hardness value (VHN) > 410 and base metal, respectively.

**Keywords** cooling rate, laser welding, reactive alloy, solidification parameter, yield point elongation

## 1. Introduction

Niobium is often termed as valve metal, which is mostly used in steels, which is added in small percentage (Ref 1) to enhance the mechanical properties of ferrous alloys. Niobium and its alloys are identified for their various combinations of properties that result into their selection for a variety of applications. In the recent time, Inconel, a nickel-based superalloy, is being replaced (Ref 2) due to the development of high-temperature structural materials like niobium and niobium-based alloy. Niobium and niobium alloy have the lowest density among all the refractory metals (Ref 3), and thus, it proves its suitability in nuclear reactors, chemical industry and aerospace applications. Increase in the flow stress when the temperature window is 800-1000 °C during the

deformation of Nb alloy affirms its stability and application as high-temperature structural material. High melting point and favorable creep strength of niobium-based alloys enable the researchers to study its suitability in the nuclear reactors (Ref 4). Ductility, relative strength and low density help niobium and niobium-based alloy to find its application in bio-engineering devices. These alloys show the property of superconductivity which can be attributed to high critical temperature when compared to other metals. Superconductivity is exhibited by niobium at the temperature of 9 K that matches with that of liquid helium temperature. It is a superconductor and therefore finds its application as a base for superconducting systems, including NbSn compounds, NbTi alloys and NbAl alloys. Niobium proves its adequacy to be used as structural material (Ref 5) in nuclear reactors as its inherent property for minimal cross-sectional area for the absorption of neutron to avoid embrittlement during service period. Zirconium application as an alloying element in the alloy used in nuclear material as structural material can be attributed to properties like hardness at elevated temperature, superior corrosion resistance and neutron cross section is quite low. The improvement in the hardness is desired for the structural material (Ref 6) which have application at elevated temperature. Zirconium also enhances the ductility of the niobium-based alloy without much of change in the weight. Zr-2.5Nb alloy is widely used as cladding material for fuel tubes (Ref 7) and as structural material for its slow creep rate, compatibility with fuel and resistance to neutronic embrittlement that results longer service life of high-pressure tubes.

Niobium is gaining importance in the field of bio-engineering (Ref 8) due to its bio-compatibility properties. Niobium also

Santosh Kumar Gupta and Sanjib Jaypuria, Advanced Technology Development Centre, Indian Institute of Technology Kharagpur, Kharagpur 721302, India; and Dilip Kumar Pratihari and Partha Saha, Department of Mechanical Engineering, Indian Institute of Technology Kharagpur, Kharagpur 721302, India. Contact e-mails: santoshduce@gmail.com, sanjibjaypuria@gmail.com, dkpra@mech.iitkgp.ac.in, and psaha@mech.iitkgp.ac.in.

finds application in several biological fields such as shape memory alloy. Titanium-based alloy which is widely used to build implants contains vanadium as its one of the constituents. However, if niobium is used in place of vanadium it results into higher corrosion resistance and improved bio tolerance. NiTi is a nickel- and titanium-based shape memory alloy; small percentage of niobium is added to reduce the cost and enhancement of properties. Niobium has favorable expansion property and satisfactory workability. Niobium addition as an alloying element in the shape memory alloys improves peak-to-peak transformation hysteresis. This improvement in hysteresis results into improvement of shape memory effect of the NiTi alloy. Moreover, corrosion resisting properties of niobium are highly superior to those of titanium and zirconium. Niobium and its different alloys are easily fabricable and embrittlement due to neutron absorption is relatively lower in comparison with other materials used in nuclear reactors. Niobium zirconium (Nb-1Zr) is a solid-solution strengthened alloy (Ref 9) having superior properties as compared to that of pure niobium. Nb-1Zr is modified by adding 0.1% of C (Ref 10) to increase the operating life and improve the high-temperature strength (Ref 11) which is required for SP100 reactors. Adequacy in nuclear environments and availability makes it a potential candidate to be used as a structural material in Compact High-Temperature Reactor, (Ref 12) aerospace engines and space nuclear reactors. High creep rupture property is one of the prerequisites for the structural material used for the building nuclear plants. It is seen from the literature that niobium-based alloy finds wider application as structural components in most of the nuclear reactors.

Titran reported that the creep test of electron beam welded joints is conducted at the temperature of 1350 K that shows fusion zone (FZ) to have better creep strength in both the conditions of heat treatment, i.e., annealing and aging (Ref 13). Kramer carried out welding of thin sheets of niobium alloy using laser and electron beam welding technique and presented that niobium weld joint failed in the HAZ when fabricated with laser. The grain size and width of the HAZ as obtained in laser welding is smaller as compared to the electron beam welding (Ref 14). Welding of niobium and niobium-based alloy is often carried out in vacuum condition, i.e., controlled condition. The fabrication of the alloy has been attempted mostly in the vacuum environment to prohibit reactivity and contamination during welding (Ref 15, 16). However, welding of niobium (Ref 17) can be carried out in the open atmosphere by using inert shield of argon or helium. Scott (Ref 18) reported that machine welding is favored over manual when open air fabrication due to better steadiness and speed of the torch can be varied leading to less contamination. Badgular (Ref 6) carried out electron beam welding of Nb-1% Zr-0.1% C and studied the effect of power and welding speed on penetration depth, weld width, aspect ratio, joining and thermal and joining efficiency. Hajitabar et al. (Ref 3) reported that the optimum level of mechanical and metallurgical properties can be attained by maintaining welding current at 30 mA during electron beam welding (EBW) of Nb-1Zr alloy. Tungsten inert gas welding is one of the popular welding techniques known for giving smooth root of the weld-bead but still it is a less preferred technique for the welding of niobium, because entrapment of air in the FZ cannot be avoided (Ref 19). Defocusing of electron beam is done to minimize the energy density and thus to achieve smooth weld root. However, a proper control of material thickness is required to avoid blowholes in the FZ.

Conventional welding techniques like gas metal arc welding (GMAW) and gas tungsten arc welding (GTAW) result in grain growth and recrystallization of heat-affected zone due to high heat input. This results into a rise of ductile to brittle transition temperature and susceptibility toward failure in the presence of cracks, notches and craters. Laser beam welding (LBW) and electron beam welding help to overcome these issues by application of low heat input (Ref 20). Gerken reported the presence of centerline cracks and micro-cracks in the FZ and HAZ, respectively, in the welded joints of niobium fabricated at high heat inputs of EBW and GTAW (Ref 21). Santella carried out welding of Nb-1Zr alloy using manual gas tungsten arc welding technique in glove box, where argon and helium are separately used as inert environment. The hardness of FZ is higher than base metal in both welded and post-weld heat-treated conditions (Ref 22). Niobium being highly reactive element toward atmospheric gases at elevated temperature, it is advisable to carry out its welding in inert environment with high purity or in vacuum to impede increase in the hardness of the FZ. Proper cleaning and edge preparation are also suggested to minimize the decrease in ductility and toughness (Ref 17, 18, 23, 24, 25). High melting point and thermal conductivity of niobium and its alloy make its welding tedious. EBW and LBW are the most preferred welding techniques over resistance and tungsten inert gas welding. These techniques ensure minimum size of FZ, HAZ and distortion with full penetration welds because of the lower heat input (Ref 26, 27, 28).

Although the vacuum environment of EBW is recommended for the fabrication of the alloy, the cost associated with the complex working environment is huge as compared to other high energy density welding processes. Welding in controlled atmosphere has less efficiency in terms number of joints made when compared to high energy density welding process like laser beam welding. In the earlier studies effect of microstructural evolution, phase changes and cooling rates on mechanical and metallurgical properties are very scanty. The effect of the dissolution of carbide precipitates depending upon the heat input during welding is unavailable in the earlier studies. Laser beam welding of reactive metals like niobium and niobium based is still less explored and requires well establishment of this autogenous welding process.

Therefore, laser welding of PWC-11 alloy has been attempted to study the viability of the process. It is also observed that there is limited literature on laser processing of the alloy, which is assumed to be undergo significant microstructural variation due to the reactive nature at elevated temperature. In addition to this, the available literature on the laser welding and strength measurement of the welded joints of Nb-1% Zr-0.1% C is limited. This encourages carrying out a study on the quantification and comparison of the strength, ductility and micro-hardness of the laser-welded joints and interpretation of the observed result in context to the laser input parameters, i.e., laser power, welding speed and beam diameter. The present study deals with effect of variation of welding speed on the mechanical and metallurgical properties of the welded joints. Precipitation behavior, grain size, morphology and cooling rate have been considered as the microstructural characterization criteria of the joint to correlate the hardness, strength and ductility of the joints.

## 2. Materials and Methods

Precipitation-strengthened Nb-1%Zr-0.1%C alloy (PWC-11) is used for carrying out LBW and other mechanical and metallurgical tests to decide the quality of the welded samples. Nb-1%Zr-0.1%C alloy is produced by the addition of zirconium and carbides in the niobium matrix according to the weight percentages mentioned in Table 1. Powders of niobium, zirconium and carbides are electron beam melted in a vacuum condition to avoid contamination by the impurities, as specified in Table 1. Electron beam melting is followed by isostatic pressing, sintering, forging, cold/hot rolling and heat treatment, i.e., annealing. Sheets with the desired properties and thickness are finally obtained after carrying out the above manufacturing processes. Bead-on-plate (BOP) welding experiments are conducted prior to the butt-welding experiments to ascertain the range of process parameters in order to attain full penetration welds. The schematic view and photograph of bead-on-plate (BOP) are shown in Fig. 1(a) and (b), respectively. Butt joints are made with the sheet dimensions of 70 mm x 20 mm x 0.5 mm, which are polished, etched and ultrasonically cleaned prior to the welding. The schematic view and photograph of butt welding are shown in Figure 1(c) and (d), respectively.

Yb-fiber laser (IPG YLR-2000) operating at 1.064  $\mu\text{m}$  and maximum power of 2 kW, located at IIT Kharagpur, India, is used to carry out the welding experiments. The power density is varied from 2.17 to 5.91  $\text{W}/\text{cm}^2$ . Pre-welding sample preparation is done by milling of the surface and edges followed by polishing of the samples, and then, these are etched using  $\text{H}_2\text{O}$ , HF,  $\text{H}_2\text{SO}_4$  and  $\text{HNO}_3$  in the ratio of 55: 22:15:8. Ultrasonic cleaning of the samples is carried out in propanol bath to decrease the samples that can result into weld defect. The different levels of input parameters used for welding of the niobium alloy are illustrated in Table 2. A suitable clamping arrangement is provided on the sides of the sheets to be welded for minimization of the distortion during welding. Shielding gas is provided on both the top surface and bottom of the weld-pool to avoid contamination of the melt pool. It is done to eliminate the possibility of oxides and nitrides formation. However, optimized argon flow is required to minimize its effect on the cooling rate and obtain proper shielding conditions during the welding process. Argon flow is maintained at 20 L/min during the welding. During the experiments, the variation of the temperature is recorded using IR pyrometer to determine the cooling rates. The pyrometer and samples are kept fixed and laser is moved to carry out the joining process. The pyrometer and the laser scanning direction are kept perpendicular to each other to capture the molten-pool thermal history. The effect of variation of welding speed on the properties of the joints can be studied by co-relating with the cooling rate. The welding speed is varied from 1000 mm/min to 1500 mm/min. A transverse surface of the welded joint is cut using wire electrical discharge machine (EDM) for the investigation of microstructure, bead profile and hardness of the laser-welded alloy. The cut

specimen from the joint is subjected to polishing with emery paper of different grits and then etched in the solution of HF,  $\text{HNO}_3$  and  $\text{H}_2\text{SO}_4$ . The concentration of HF,  $\text{HNO}_3$  and  $\text{H}_2\text{SO}_4$  is maintained in the ratio of 1:1:3. Etching is followed by ultrasonic cleaning in 2-propanol bath to reveal microstructure. Scanning electron microscope (SEM) (EVO 15, Zeiss, Jena, Germany) coupled with EDAX (AMETEK) helps in capturing microstructure and estimation of elemental distribution in the weld zone. X-ray diffractometer (PANalytic Empyrean Cu LFF HR (9430 033 7310x) DK411025, Netherlands) generating  $\text{Cu K}\alpha$  radiation helps in identification of the phases present in the fusion zone and in the base metal. Hardness tester (OMNI-TECH MVH-S-AUTO) is used to estimate the variation in hardness of base metal (BM), heat-affected zone (HAZ) and fusion zone (FZ) measured at 50 gf at dwell time of 10 s. The tensile samples are cut from the welded sample and base metal using EDM of the dimensions given in Fig. 2. Tensile samples are sub-sized, designed by maintaining ASTM E8. The strength measurement was done INSTRON. The cross-head speed is maintained at 0.2 mm/min for carrying out tensile tests for both the welded and base metal.

## 3. Results and Discussion

### 3.1 Cooling Rate and Molten Pool Thermal History

Welding speed is the key parameter to affect the cooling rate and molten pool's life time. In Fig. 3, the curve OP is the time duration for creating molten pool during the heating cycle. As the laser advances away, we obtain the curve PC, which describes the cooling cycle of trailing molten pool created by high density laser source irradiation of laser. The molten pool's life time is calculated from P to E. Nucleation initiates from the point D, as depicted in the curve, and DE is the region of solidification of the molten pool. In Fig. 3, during the cooling cycle, there are two solidification shelves, i.e., A and B, and this is due to different alloying elements of Nb-1% Zr-0.1% C with different melting points. The nucleation of the molten pool starts from A and ends at B.

In Fig. 4(a), (c) and (e), thermal history of three welds obtained with welding speed of 1000, 1250 and 1500 mm/min is plotted by keeping the laser power and laser beam diameter constant, respectively. The cooling rates of the three different combinations of input parameters are given in Table 3. It is quite obvious from the data that the cooling rate increases with increase in the welding speed, which controls linear heat input per unit length during welding. Aspect ratio values are also found to be increasing with the increase in welding speed. A lower welding speed always enhances the probability of plasma formation, which contributes for a shallow bead profile and results in reduction of aspect ratio. Plasma formed during welding is also responsible for the material removal and ultimately, thinning of the weld zone of the samples. Thinning of these samples due to plasma causes reduction in strength of the joint. In addition to this, the high conductivity of niobium alloy causes significant lateral melting during welding with the low speed. Niobium alloy with inherent high conductivity and thickness of 0.5 mm results in significant lateral heat transfer, and therefore, undesirable weld profile is obtained after the welding.

**Table 1** Composition Nb-1Zr-0.1C of alloy

Zr, wt%	C, wt%	Impurities, ppm	Nb, wt%
0.9-1.2	0.1-0.13	H-4, N-41, O-132	Balance

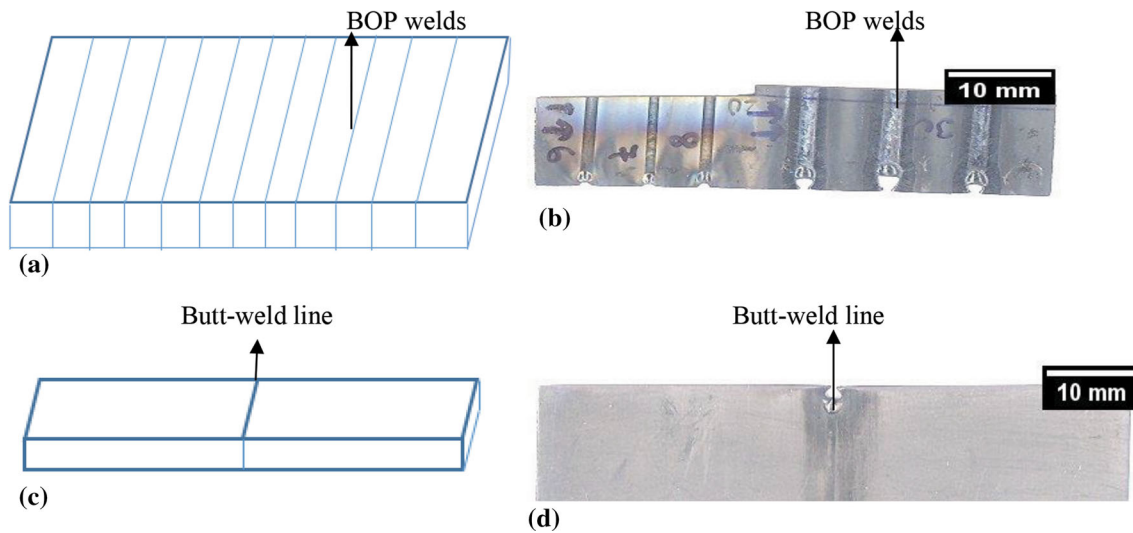


**Fig. 1** (a) Schematic view of experimental specimen for BOP laser welding, (b) photograph of BOP laser-welded niobium alloy sheet, (c) schematic view of experimental specimen for butt laser welding and (d) photograph of butt laser-welded niobium alloy sheet

**Table 2** Experimental runs with response parameters for continuous wave mode

Input parameters	Level 1	Level 2	Level 3
Laser power, Watt	1200	1450	1700
Welding speed, mm/min	1000	1250	1500
Beam diameter, mm	0.66	0.72	0.82

Thermal history of molten pool and cooling rate are the key factors in determining the mechanical and metallurgical properties. Therefore, further assertion on mechanical and metallurgical properties of FZ will be primarily based on the thermal cycles and cooling rate experienced by the weld. Figure 4(b), (d) and (f) shows the different grain morphologies evolved in FZ due to different welding speeds or cooling rates. Grain refinement is experienced with an increase in the welding speed. With the increase in welding speed in the experiments, the interaction time of the laser with samples decreases, and therefore, the peak temperature decreases. However, when the temperature profile of the experiment welded with input parameters of 1450 W, 1500 mm/min and 0.66 mm is analyzed, it is observed that there is very less variation of the peak temperatures obtained with 1450 W, 1250 mm/min and 0.66 mm. This small variation between the peak temperatures can attribute to the formation of the new phase  $Nb_6C_5$ , which is confirmed in the phase analysis, as discussed above. The enthalpy of the formation of  $Nb_6C_5$  is less, and it is more exothermic than other two carbide phases, i.e.,  $NbC$  and  $Nb_2C$ . Therefore, the formation of  $Nb_6C_5$  phase results in the increase in peak temperature during the welding.

### 3.2 Effect of the Input Parameters on the Mechanical Properties

Hardness variation is found to be quite abrupt, when we compare the values observed in the base metal and in the FZ. Micro-hardness of FZ varies from 2.5 to 5 times higher than that of the base metal. The input-output modeling of the

experiments is carried out to study the significance of the process parameters on the results. In the present study, the effect of laser power, welding speed and beam diameter is studied on the hardness of the fusion zone. It is observed from Table 4 that the effect of welding speed and beam diameter on the hardness of the FZ is quite pronounced. The variation of the hardness with the increase in laser power presents an increasing trend up to mid value and then a decreasing trend. However, individual contribution of laser power is not significant. Therefore, the combined effect of laser heat input is taken into consideration. When individual effect of the process parameters is studied from Fig. 5, hardness increases with an increase in velocity, due to increase in cooling rate. As cooling rate increases, there is grain refinement, and thus, hardness improves in the FZ (Ref 35, 36, 37). Hardness decreases with an increase in beam diameter, as seen from Fig. 5. This increase in beam diameter results in lowering of energy density (Ref 38), and therefore, hardness reduction is observed. The squared coefficient of correlation is found to be 0.89 for regression-based prediction of hardness with respect to input parameters. Minitab 15 (Ref 40) is used to obtain the regression Eq 1, which shows the mathematical dependence of hardness (Ref 39) on laser power, welding speed and beam diameter.

$$FZ(VHN) = 615 - 0.0301 \times P + 0.275 \times V - 759 \times D \quad (\text{Eq 1})$$

The reduction of the elongation, yield and ultimate strength of the welded joints is experienced, when it is compared to that of the parent metal's properties. The welding parameters have significant contributions on the limit of the elastic and plastic regime. when the effects of the welding parameters are studied on the yield strength, tensile strength and elongation and are presented in Tables 5, 6 and 7. It can be concluded that laser power is insignificant in all responses, as per the ANOVA results. In the present study, welding speed and beam diameter are found to have significant contributions for the outputs, i.e., YS, UTS and El. The regression Eq. 2, 3 and 4 relate laser power, welding speed and beam diameter with YS, UTS and elongation, respectively. The squared coefficient of correlation is found to be equal to 83.9, 87.1 and 88.4% for the yield

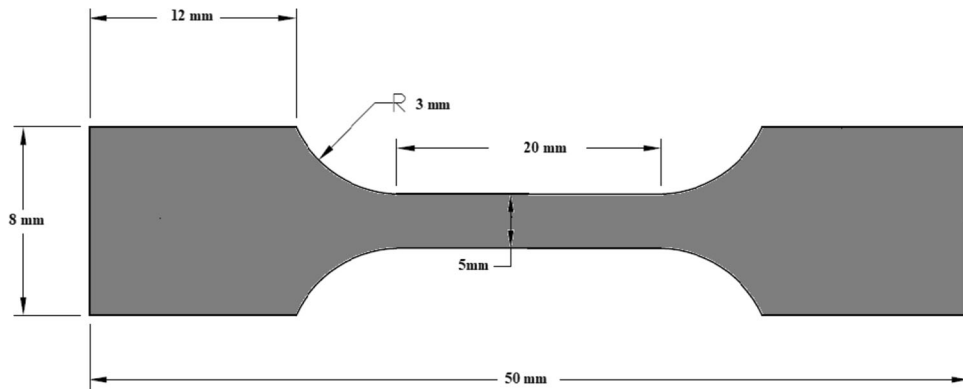


**Fig. 2** Schematic view of tensile sample for uniaxial testing

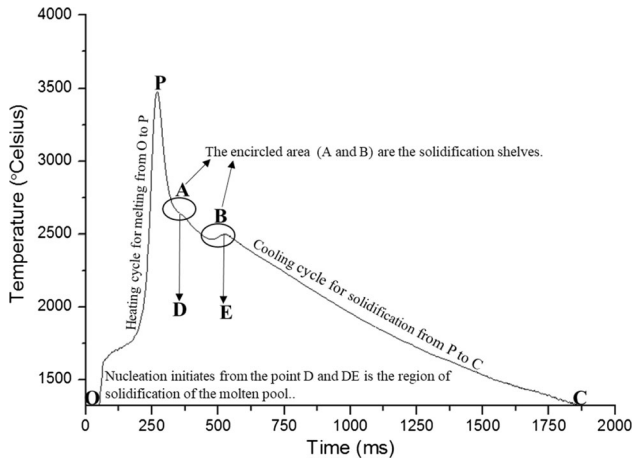


**Fig. 3** Thermal cycle for the fusion zone when welded using input parameters: 1450 W, 1000 mm/min, 0.66 mm

strength, ultimate strength and elongation, respectively. The observed values of squared coefficient of correlation signify that the regression modeling is acceptable and can predict the outputs with less deviation from the original value.

$$YS = 221 - 0.00103 \times P + 0.0146 \times V - 24.3 \times D \quad (\text{Eq } 2)$$

$$UTS = 235 + 0.0140 \times P - 0.126 \times V + 309 \times D \quad (\text{Eq } 3)$$

$$EI = -0.40 + 0.00086 \times P - 0.00852 \times V + 19.2 \times D \quad (\text{Eq } 4)$$

Figure 6 depicts the variation of YS, UTS and EI depending upon the variation of process parameters. It is found from Fig. 6 (a) that yield strength increases initially up to the middle level of laser power and then decreases. There is no significant variation in the mean plot for yield strength with respect to the laser power and it resembles the same trend as that observed in the variation of hardness. However, when we consider dependence of yield strength on the welding speed, yield strength shows a step rise with increase in welding speed due to an increment in the cooling rate. Beam diameter holds an inverse relationship with yield strength. The larger the value of beam diameter, the smaller is the energy density and it leads declination in yield strength value of the joints. The results of yield strength can be attributed to the hardness of fusion zone in

the joints. The higher the value of hardness in FZ of the welded sample, the higher will be the value of yield strength in the welded joints.

In Fig. 6 (b) and (c), it is evident that ultimate tensile strength and elongation are observed to be decreasing up to the mid-level of laser power due to increase in heat input, which favors grain refinement to some extent, but it improves at the higher level of laser power. The variation of tensile strength and ductility presents an inverse relation with welding speed. Beam diameter has integral relation with the plasticity and tensile strength of the welded joints. With the increase in the beam diameter, the heat concentration over a small area decreases, which minimizes the heat input, and thus, we obtain the better strength and improved ductility.

The increase in the hardness and yield strength greatly affects the ultimate strength and permanent elongation of the welded joints. In order to maintain proportionality between yield strength, tensile strength, ductility and hardness, the process needs to be optimized as per the industrial requirement. This kind of optimization can be solved for a suitable hardness value in the weld part without sacrificing strength and ductility of the joint.

It can be concluded from the above the study that welding speed plays a significant role followed by beam diameter in determining the mechanical and metallurgical properties. However, variation of beam diameter has minimum significance on the variation of the responses as compared to the welding speed. Therefore, the study is carried out based on the effect of the variation of the welding speed on the mechanical as well as the metallurgical properties.

### 3.3 Phase Analysis of the Base Metal and Welded Samples

Figure 7 depicts the x-ray spectra as obtained for the base metal and welded samples fabricated with the welding speed of 1000, 1250 and 1500 mm/min. The other two input parameters, i.e., laser power and beam diameter, are kept constant to capture the effect of welding speed on the phase evolution in the FZ during welding. The main objective of the study is to determine the different phases formed in fusion zone and to correlate the mechanical properties with formed different brittle phases. The base metal is mainly composed of the phases Nb, Zr, C, Nb<sub>2</sub>C, Nb<sub>2</sub>O<sub>5</sub>, ZrO, ZrC and Nb<sub>2</sub>N. The FZ of the welds joined using welding speed of 1000 and 1250 mm/min does not show any new carbides as compared to base metal. However, different phases of nitrides and oxides of niobium are found to be formed during welding. The formation of nitrides and oxides of

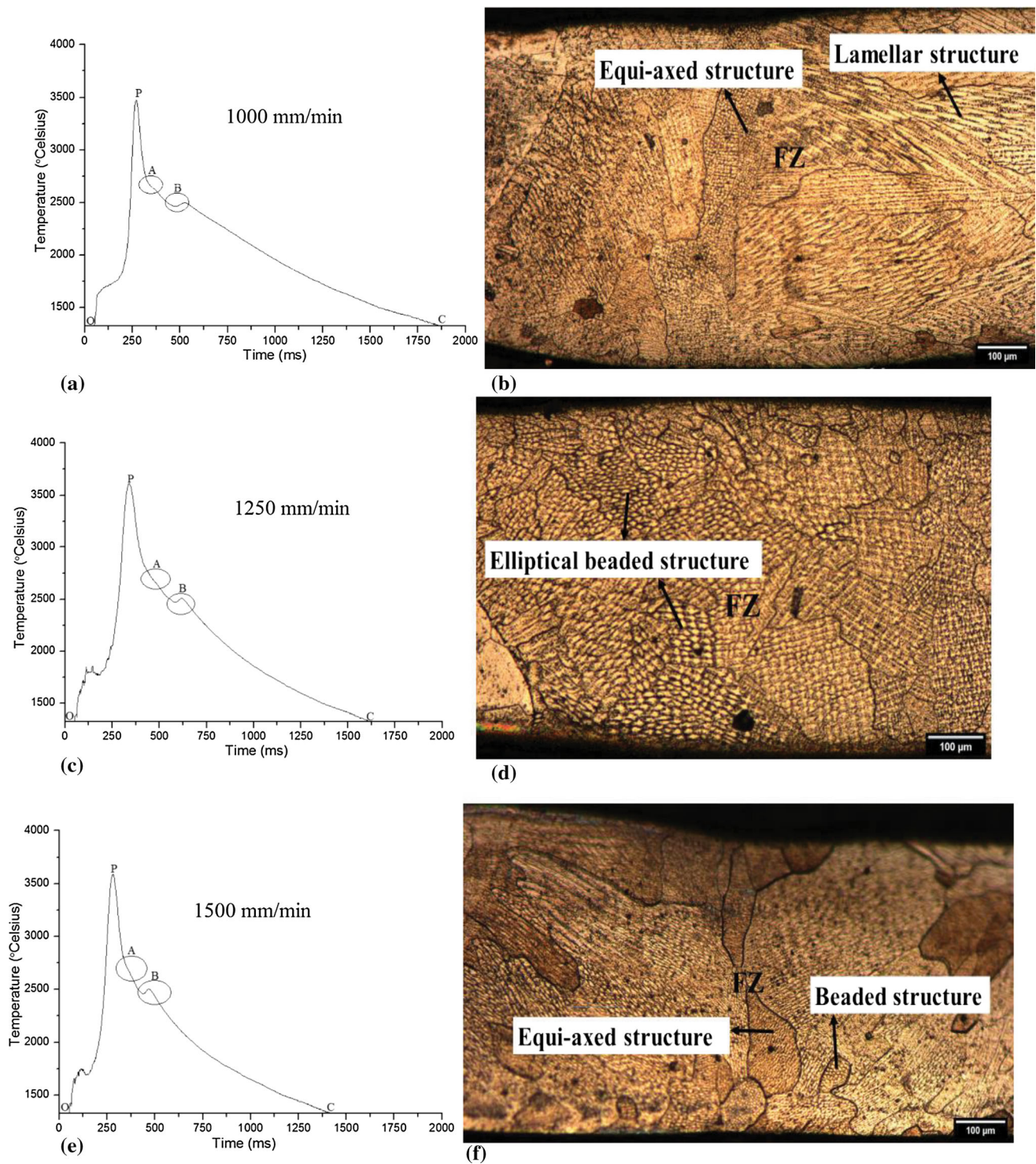


**Fig. 4** Thermal cycle and microstructure evolution in FZ welded with varying welding speeds

**Table 3** Aspect ratios and cooling rates for different combinations of input parameters

Sr No.	Laser power, P, Watt	Welding speed, V, mm/min	Beam diameter, D, mm	Aspect ratio	Cooling rate, °C/ms
1	1450	1000	0.66	0.25	492.9
2	1450	1250	0.66	0.27	611.8
3	1450	1500	0.66	0.32	645.4

**Table 4 ANOVA results for hardness**

Predictor	Coef	SE Coef	T	P
Constant	614.6	103.6	5.93	0.000
Laser power	-0.03011	0.03643	-0.83	0.423
Welding speed	0.27487	0.03643	7.55	0.000
Beam diameter	-758.8	105.3	-7.21	0.000

**Table 7 ANOVA results for elongation**

Predictor	Coef	SE Coef	T	P
Constant	-0.400	3.115	-0.13	0.900
Laser power	0.000860	0.001095	0.79	0.446
Welding speed	-0.008516	0.001095	-7.77	0.000
Beam diameter	19.157	3.166	6.05	0.000

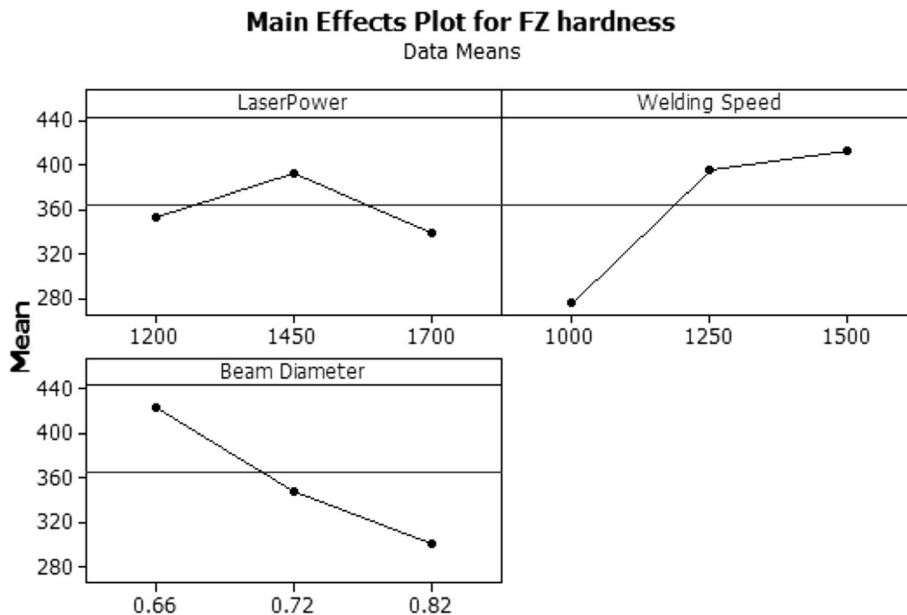


**Fig. 5** Main effect plot for hardness of the fusion zone

**Table 5 ANOVA results for yield strength**

Predictor	Coef	SE Coef	T	P
Constant	220.709	5.838	37.81	0.000
Laser power	0.001032	0.002053	-0.50	0.624
Welding speed	0.014600	0.002053	7.11	0.000
Beam diameter	-24.334	5.932	-4.10	0.000

**Table 6 ANOVA results for ultimate tensile strength**

Predictor	Coef	SE Coef	T	P
Constant	235.48	50.20	4.69	0.000
Laser power	0.01397	0.01765	0.79	0.443
Welding speed	-0.12575	0.01765	-7.12	0.000
Beam diameter	308.98	51.02	6.06	0.000

niobium can be attributed to open atmospheric working condition during laser welding of reactive niobium alloy. The formation of these oxides and nitrides is a reason for the increase in the hardness of the FZ and depletion in the strength of the welded joints. There is also formation of ZrO<sub>2</sub> in the FZ of the welds joined with three different welding speeds. Zirconium is added in the niobium matrix to get oxygen and help in reducing the possibilities of formation of oxides of

niobium. However, when the FZ of the weld joined using the welding speed of 1500 mm/min is analyzed, there is formation of two new phases of carbides of niobium. These two phases are NbC and Nb<sub>6</sub>C<sub>5</sub>, which have been reported (Ref 29) as significant contributors for the enhancement of hardness and depletion of ductility in the welded joints. The formation of new carbides of niobium is on the expense of dilution of Nb<sub>2</sub>C. Nb<sub>2</sub>C is the stable carbide phase of the niobium imparting good properties to the niobium-based alloy (Ref 30). The most catastrophic oxide of niobium formed in the weld of 1500 mm/min is Nb<sub>2</sub>O<sub>5</sub>. This oxide is brittle and porous, which cannot act as layer on the surface of the niobium alloy to protect the corrosion (Ref 31). The formation of new layer of Nb<sub>2</sub>O<sub>5</sub> follows a parabolic curve, when the temperature is increased from room temperature toward the application temperature of 1000°C. The formation of new layer of oxide of niobium results in the degeneration of the thickness and thus decreases the lifetime of the niobium alloy in the application area. High heat input prohibits the formation of phases that deteriorate the desirable properties.

**3.4 Microstructure and Hardness of the Base Metals and Weld-Bead Welded in Continuous Wave Mode**

Fusion zone of all weld samples exhibits an increase in hardness, and a sharp reduction of hardness is observed in the heat-affected zone (HAZ). The aberration of the average hardness of the base metal and FZ is quite steep. Increase in hardness can be attributed to the variation of grain size in FZ, as

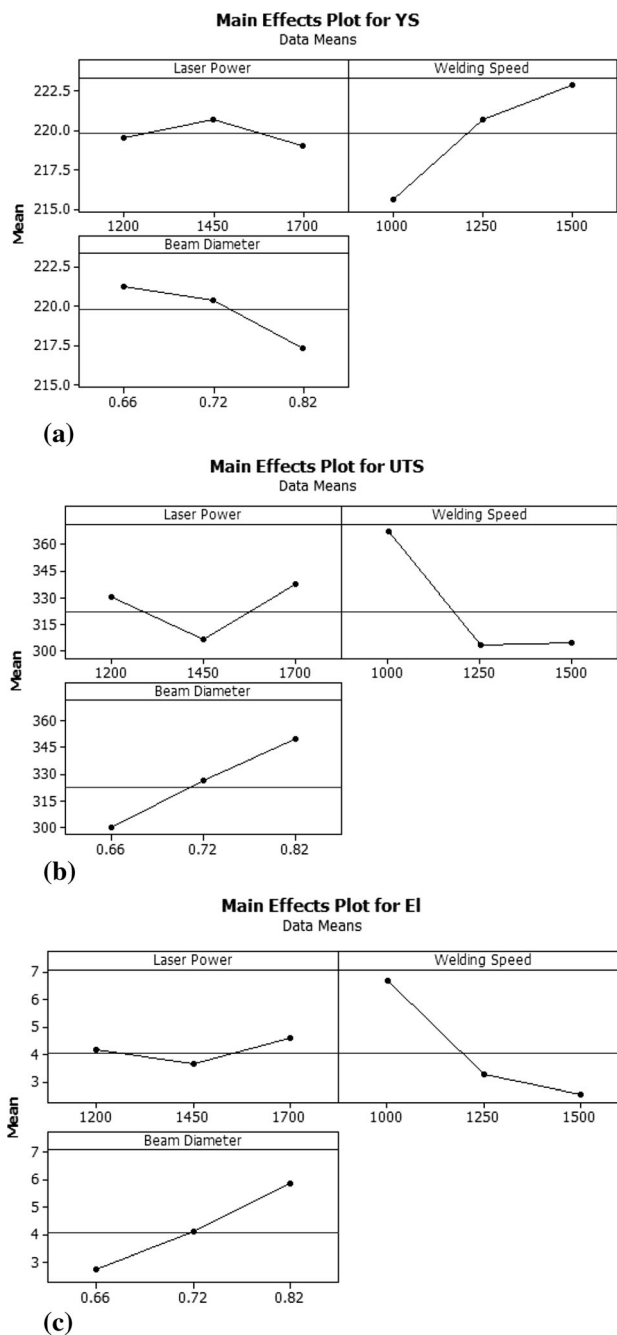


**Fig. 6** Main effect plot for (a) yield strength (b) ultimate tensile strength and (c) elongation

compared to that of unwelded zone. The fusion zone of most of the samples consists of fine equi-axed grains. The size of these fine equi-axed grains varies in between 1 and 2  $\mu\text{m}$ . Equi-axed grains are mainly found at the center of the fusion zone. As we move toward the HAZ, bead-like structures are observed. These bead-like structures are present in the region away from the center of FZ. The size of bead-like structures varies in the range of 5-10  $\mu\text{m}$ . Elliptical bead-like structures and lamellar structures are evitable near the HAZ. These micro-features measure 10-15  $\mu\text{m}$  and 20-22  $\mu\text{m}$  in size. Elliptical bead-like structures and lamellar structures are mainly observed in the weld zone of samples having ductile mode of failure during the uniaxial tensile tests. Depending upon the size of the grains

found in the FZ, individual grains have different local plastic strength or hardness. The hardness values of the FZ joined with different heat input are tabulated in Table 8.

The grain size of the welds is dependent on the welding speed/cooling rate, solidification parameter ( $(G/R)$ ), where  $G$  is thermal gradient and  $R$  is the measure of rate of the advancement of solidification front, nucleation of grains and undercooling. The joints having the finer grains, such as equi-axed and beaded structures, appear as to be arranged. The grain size gets smaller with the welding speed, as the interaction time of laser source decreases and thereby increases the rate of heat transfer. Enhanced cooling rate helps in increased rate of heat dissipation, and overall nucleation of grains is more. The amount of undercooling also controls the formation of equi-axed grains. The amount of undercooling is more in the experiment carried out at the welding speed of 1500 mm/min, as shown in Fig. 4 (e). The solidification parameter ( $(G/R)$ ) is the ratio of melting temperature ( $T_M$ ) and the product of welding speed ( $V$ ) and distance between the laser source (O) and tail of the melt pool ( $a_1$ ), as given in Fig. 8. The solidification parameter is calculated from Eq 5 that determines the grain morphology. With the increase in the welding speed, the distance  $a_1$  increases, and thus, solidification parameter value decreases. The decrease in solidification parameters and nucleation helps in the formation of equi-axed grains. Thus, equi-axed grain morphology is controlled by increased cooling rate, nucleation of grains and undercooling and decreased in solidification parameter.

$$G/R = \frac{T_M}{V \times a_1} \quad (\text{Eq 5})$$

The microstructure of the weld joined at the welding speed of 1000 mm/min has equi-axed and elliptical grains. The elliptical shape has its semimajor axis aligned in the perpendicular direction of the laser scanning direction or horizontal to the transverse direction. The growth of grain along the perpendicular direction to the scan direction can be attributed to the heat transfer occurring along the width of the niobium sheet to be welded. The sheets to be joined are 0.5 mm in thickness, and therefore, very much less thermal gradient can be attained along the thickness, which controls the grain structure. Minimal difference in the size of the elliptical grains supports the fact of less gradient in temperature along the thickness. Niobium having high melting point and thermal conductivity requires high level of laser power for welding. This results in the rise of temperature of around 3500°C in the FZ. The thermal gradient is quite large in between the base metal and FZ. Conduction being dominant mode of heat transfer when the thermal gradient is high, the dissipation of heat from the material occurs largely from base metal, and hence, the grain direction is kept along the traverse direction.

The enhanced hardness in the FZ can also be attributed to brittle hard phases formed owing to the intense local heat during the laser welding of Nb alloy. The significance of individual parameters can be analyzed by varying that parameter and keeping the other two process parameters constant. Figure 11 depicts the hardness of the FZ and HAZ of the samples welded with different combinations of the input parameters. From the analysis of the hardness values, it can be concluded that welding speed has the significant contribution on the hardness of the FZ. Due to high welding speed, the FZ experiences high thermal gradient in short duration of time,



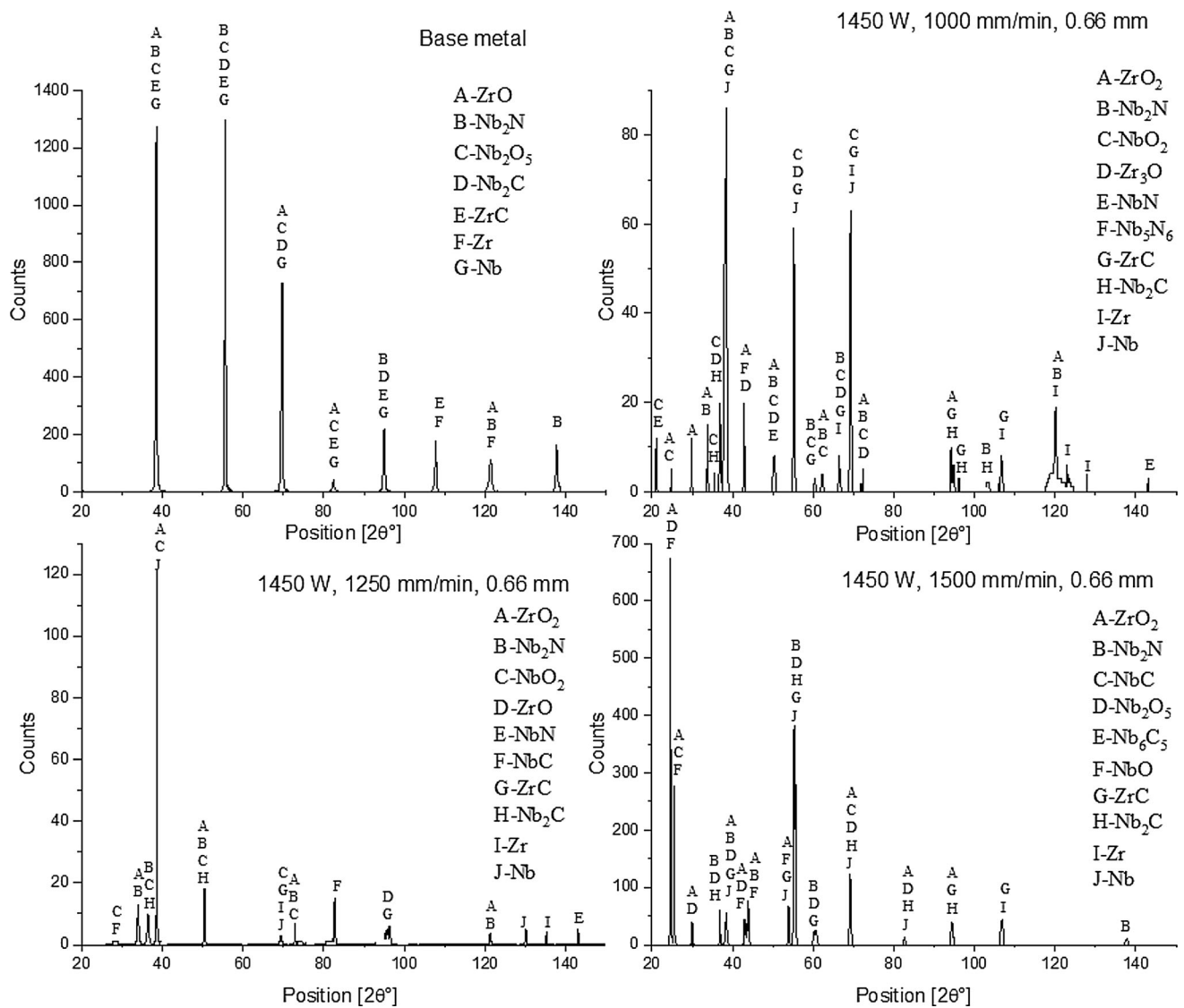


Fig. 7 XRD phase pattern for the (a) base metal (b) 1450 W, 1500 mm/min, 0.66 mm, (c) 1450 W, 1250 mm/min, 0.66 mm and (d) 1450 W, 1500 mm/min, 0.66 mm

Table 8 Average micro-hardness of the weld zone welded at different heat input

Sr. No.	Laser power, P Watt	Welding speed, V, mm/min	Beam diameter, D, mm	Heat input, KJ/mm	Micro-hardness VHN
1	1450	1000	0.66	89.99	332.90
2	1450	1250	0.66	69.60	425.10
3	1450	1500	0.66	58.00	521.60

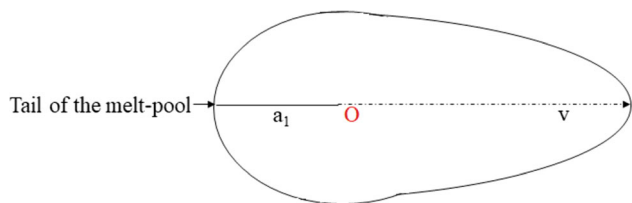


Fig. 8 Illustration of melt pool

i.e., cooling rate is quite pronounced. FZ experiencing high cooling rate results in refinement of grains. The grain size gradually increases from the center of the FZ toward the base metal (Ref 32, 33). As a result of increase in the grain size, there is a decrease in the hardness. Figure 9 depicts the optical images of the welded sample. The variations of the constituent elements of the alloy in the FZ, HAZ and base metal are depicted in Figure 10. The variation of hardness from the weld centerline toward base metal in the welds of niobium alloy is illustrated in Fig. 11. The spots: 1, 2 and 3 are the EDS points located in the FZ, HAZ and base metal, respectively. The

percentage increase in the carbon and oxygen can be associated with the formation of the carbide and oxide phases of niobium, which is responsible for the improved hardness in the FZ and HAZ (Ref 34). The hardness values of different grain structures present in the molten zone are displayed in Table 9. The average hardness value of base metal (BM) is found to be around 110 VHN and that of FZ lies in between 252.7 and 538.5 VHN. The substantial increase in the hardness is mainly due to the formation of NbC phase. Carbide dissolution takes place due to the laser heat confined to small area and this carbide bonds with Nb<sub>2</sub>C to form metastable NbC at the time of

welding. The variation of carbide precipitate in FZ and base metal can be observed in Fig. 12 (a) and (b). The evolution of phase Nb<sub>6</sub>C<sub>5</sub> in the sample welded with a speed of 1500 mm/min further contributes in the enhancement of the hardness and brittleness of the FZ. The carbides of niobium, i.e., Nb<sub>2</sub>C < NbC < Nb<sub>6</sub>C<sub>5</sub>, present an increasing trend in the hardness.

### 3.5 Tensile Strength of the Joints Welded in Continuous Wave Mode

The welded samples exhibit reduction in the strength and ductility, as compared to that of base metal. The considered input parameters have a significant contribution in the loss of the strength and overall elongation (El) of the joints. The present study is carried out to analyze the effects of the process parameters, i.e., laser power, welding speed and beam diameter on the tensile strength, mode of failure and elongation of the laser-welded joints. The process parameters consist of three variables, which are varied over three levels to weld butt joints

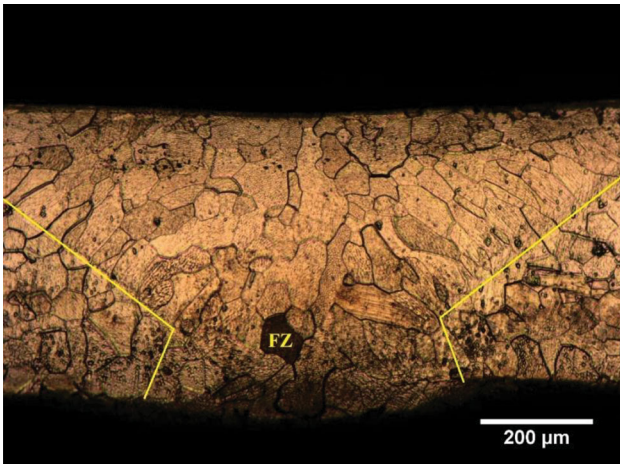


Fig. 9 Optical micrograph of welded alloy

Table 9 Micro-hardness values for different grain morphology obtained in FZ

Type of grain morphology	Micro-hardness (VHN)
Equi-axed structure	500-521
Beaded structures	400-490
Elliptical bead structures	340-400
Lamellar structure	250-340

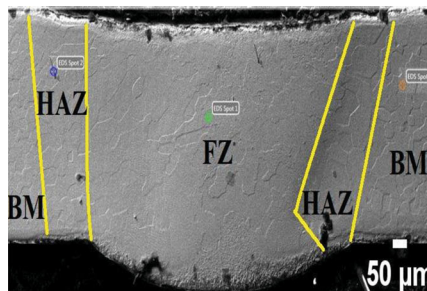


Fig. 10 EDS analysis of the FZ, HAZ and base metal

Elements (Wt. %)	Spot 1	Spot 2	Spot 3
Niobium	74.53	75.51	78.27
Zirconium	1.15	1.34	1.52
Carbon	14.07	13.92	12.30
Oxygen	4.32	3.13	3.01

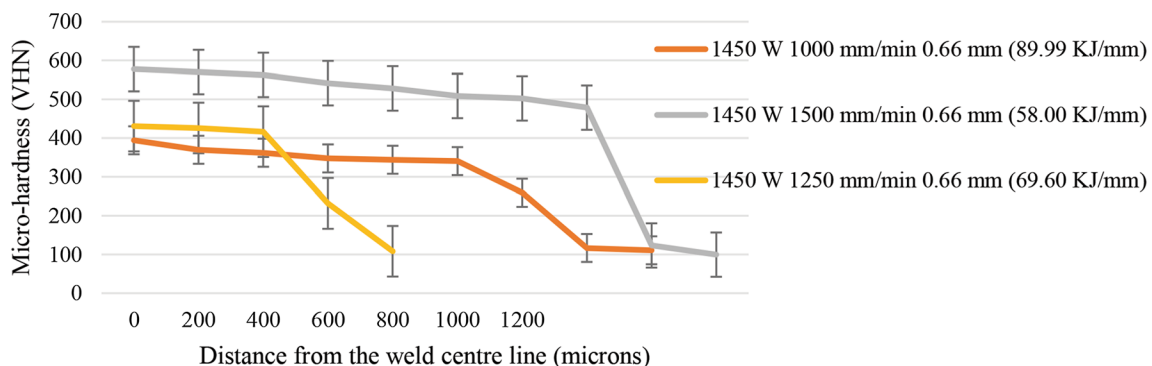
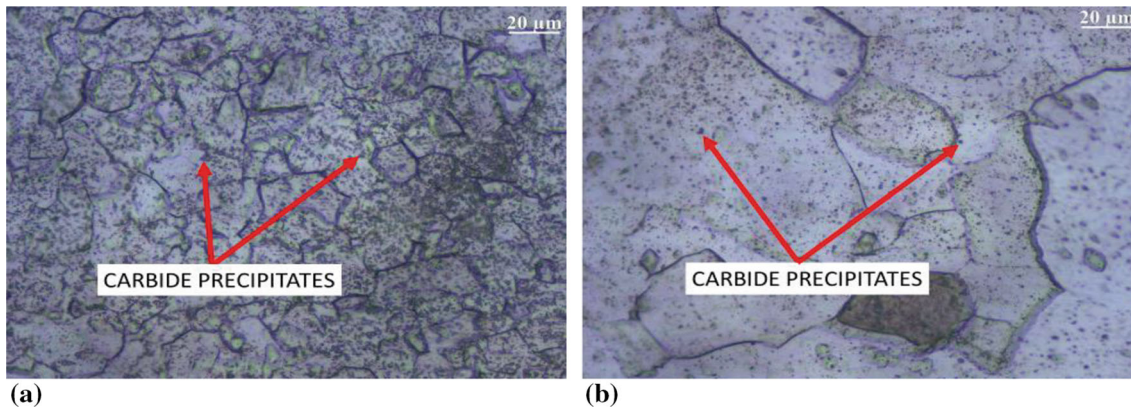


Fig. 11 Variation of the micro-hardness from the weld centerline in CW mode



**Fig. 12** Needle like carbon precipitate in (a) PWC-11 alloy base metal, and (b) fusion zone of PWC-11 alloy

of size 70mm X 20mm X 0.5mm. An excess flow of gas can lead to high hardness of the FZ and thus lead to brittle mode of failure.

The available literature on the laser welding and strength measurement of the welded joints of Nb-1% Zr-0.1% C is limited. This encourages for carrying out a study on the quantification and comparison of the strength and ductility of the laser-welded joints and interpretation of the observed result in context to the input parameters. Nb-1% Zr-0.1% C is precipitation-strengthened alloys, containing carbides as strengthening element in the niobium matrix. Carbides are added in the matrix, as it improves the strength of the alloy at high temperatures, i.e., 1000°C-1200°C. It improves the yield strength of the alloy, as it hinders the movement of the dislocations during deformation. Precipitation strengthening increases the stress required for a dislocation line to overcome this precipitation. Figure 13 represents encircled region, i.e., S, which signify the precipitation strengthening during the uniaxial tensile tests carried out at room temperature. S presents the serration marks caused due to the rise and fall of the stress levels at the time of tests being carried out. Increase in stress is encountered, as the movement of dislocation is hindered by the carbide precipitates. The dislocation lines move either by breaking the precipitates or by passing the hindrance caused by these interstitial elements, thereby stress level increases. This phenomenon is followed by the decrease in stress level until and unless another obstacle is encountered by the dislocation lines. The regions: S is termed as yield point elongation that helps in the improvement of yield strength. The deformation during the yield point elongation is not uniform. As discussed above, there is dissolution of the carbides due to the intense heat of the laser irradiation during the welding of the alloy. By comparing the serration marks, it can be observed that there is a decrease in the serration marks in welded specimen due to the dissolution of precipitates of carbides as compared to base metal. Decrease in the serrations marks can be attributed to the dissolution of the carbides in the FZ. The formation of the phase NbC, which is a result of carbide dissolution, has an adverse effect, as it decreases the effect of yield point elongation. In addition to this, NbC is known for the hardness and brittleness raiser and it leads to a sudden failure of the joints, which may be catastrophic in nature.

Welding speed has a significant contribution on the hardness of the FZ. The grain morphology evolution in FZ is dependent on the scan speed of the laser irradiation. The fine grains are

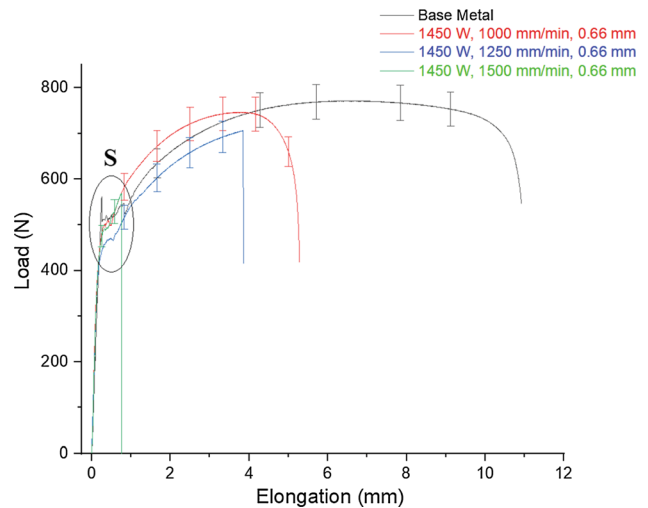


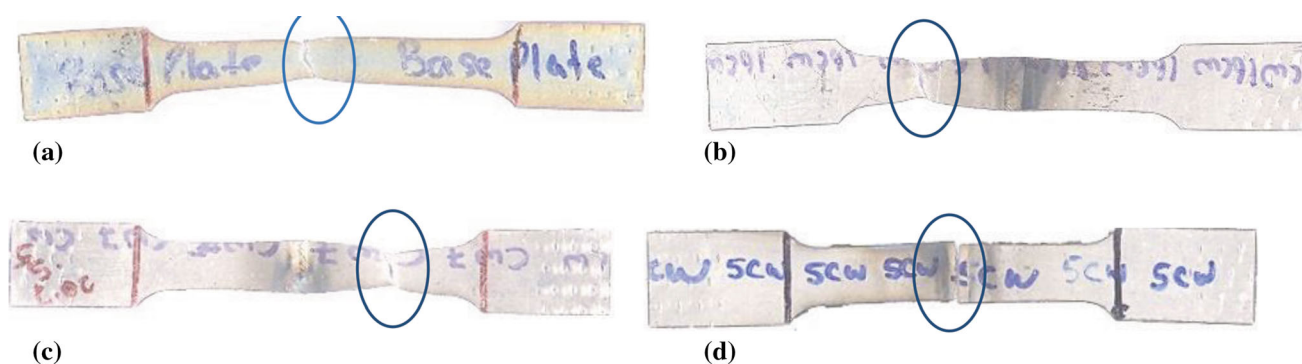
**Fig. 13** Load vs. elongation curve of Base metal and Welded samples

formed in the FZ due to high welding speed. Fine grains possess a distinctive property of high hardness. As the grain size decreases, the boundary length also tends to decrease, which, in turn, does not allow dislocation line to move out of the grains. This, in turn, causes dislocation lines to pile up at the grain boundaries and the sample experiences improvement in the yield strength. However, the sample undergoes brittle fracture, as there is a loss of ductility. The desired property is achieved in welding by maintaining an equivalence between yield strength and ultimate strength. Table 10 presents the results of the tensile tests carried out for strength analysis of the welded as well as base metal. In Fig. 13, the load vs. extension curves are plotted for the base metal and of the welded samples, where the laser power and beam diameter are kept constant at 1450 W and 0.66 mm, respectively, and the welding speed is varied as 1000 mm/min, 1250 mm/min and 1500 mm/min. It is obvious that hardness has a significant contribution on the strength and ductility of the welded joints.

The increase in the welding speed improves the hardness of the FZ, and thereby, there is a loss of ductility and tensile strength. Decrease in strength can be interpreted from the decrease in the area under plastic deformation curve, as depicted in Fig. 13. The highest elongation is obtained in the

**Table 10 Experimental runs and tensile test results**

Sl. No.	Laser power, P, Watt	Welding speed, V, m/min	Beam diameter, D, mm	Yield strength, YS, MPa	Ultimate tensile strength, UTS, MPa	Elongation, El, mm
1	1450	1250	0.66	223.30	299.51	3.73
2	1450	1000	0.66	215.45	335.96	5.47
3	1200	1000	0.82	213.01	368.44	6.76
4	1700	1500	0.82	219.25	335.76	4.67
5	1450	1250	0.82	217.56	323.69	5.63
6	1700	1500	0.72	224.30	290.0	1.41
7	1200	1000	0.72	217.50	366.39	6.64
8	1450	1250	0.72	220.62	310.90	3.92
9	1200	1500	0.72	223.22	285.56	1.20
10	1700	1000	0.72	216.14	378.71	7.43
11	1700	1000	0.82	215.81	387.05	7.68
12	1200	1500	0.82	221.13	334.64	4.58
13	1700	1250	0.66	219.40	294.66	1.68
14	1200	1250	0.66	222.63	296.23	1.54
15	1450	1500	0.66	226.50	276.21	0.76
16	1450	1250	0.66	218.83	295.79	3.12
17	1450	1250	0.66	222.40	302.34	3.30
18	Base metal			249.50	375.10	11.15

**Fig. 14** Failure location (a) base metal, (b) 1450 W, 1000 mm/min, 0.66 mm, (c) 1450 W, 1250 mm/min, 0.66 mm, and (d) 1450 W, 1500 mm/min, 0.66 mm.

welds joined with the lowest welding speed. However, there is loss of ductility and yield strength, which can be accounted to the increase in hardness and phase changes occurring in the FZ. The failure location of the base metal and welded samples are shown in Fig. 14. By keeping the laser power and laser beam diameter at 1450 W and 0.66 mm, respectively, the welded samples obtained by varying the welding speed (that is, 1000 mm/min, 1250 mm/min) have yielded the better strength compared to the parent metal, and failure zone is formed to be located in the base metal. However, the sample joined with the welding speed of 1500 mm/min has failed in the FZ.

The fractured surface of the welded samples with welding velocity of 1000, 1250 and 1500 mm/min is shown in Fig. 15(b), (c) and (d), respectively. The joints obtained with the welding speeds of 1000 mm/min and 1250 mm/min present ductile mode of failures, and the brittle mode of fracture is observed in the fractographs of joints welded with the welding speed of 1500 mm/min. It is observed that high heat input imparts ductility to the welded sheets. The joints welded with heat input of 89.99 and 69.60 KJ/mm have ductile failure, whereas the joint welded with low heat input has brittle failure.

The fractured surface of the base metal and welded samples joined with the welding speeds of 1000 and 1250 mm/min present dimple-like structures. These dimples, as observed in Figure 15(a), (c) and (d), are the spherical micro-voids that act as the center point for the initiation of the crack. The extent of ductility can be interpreted by analyzing the size of the dimples. Since base metal has the highest ductility followed by the joints welded with welding speeds of 1000 and 1250 mm/min, the dimple size decreases in the same order. The size of the dimple signifies the extent of plasticity a sample has endured, before the failure or fracture occurs. The fractured surface of the welded samples with the welding speed of 1500 mm/min depicts trans-granular mode of fracture.

#### 4. Conclusion

Nb-1%Zr-0.1%C alloy sheets are laser welded with different combinations of input parameters, and the effects of process parameters on the mechanical and metallurgical properties have

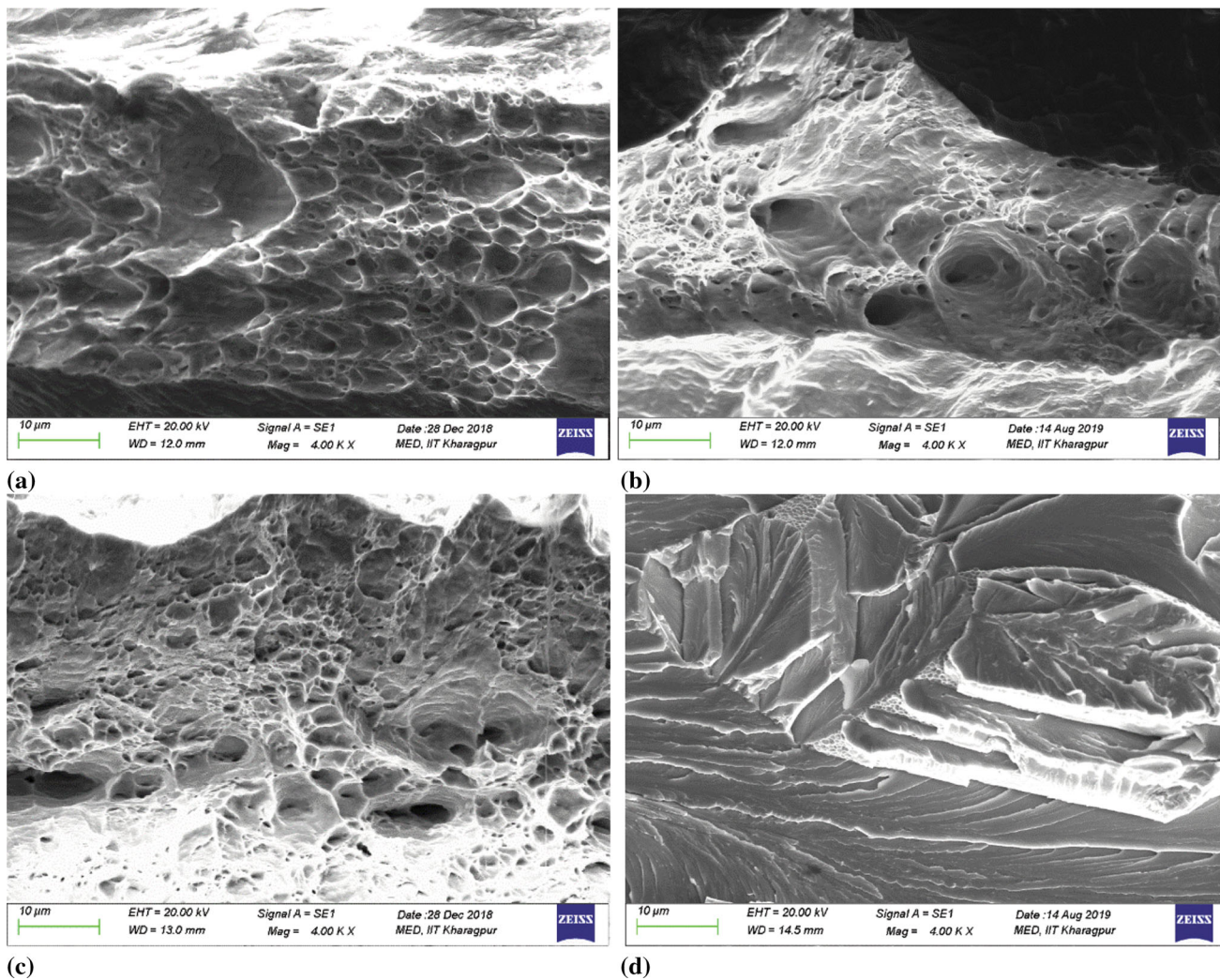


**Fig. 15** Fractured surface of (a) base metal, (b) welded at 1450 W, 1000 mm/min, 0.66 mm, (c) welded at 1450 W, 1250 mm/min, 0.66 mm, and (d) welded at 1450 W, 1500 mm/min, 0.66 mm

been studied. The following conclusion can be drawn from the study.

1. High level of heat input imparts adequate strength and ductility to the welded joints. Samples welded at high level of laser power and welding speed have presented desirable metallurgical and mechanical characteristics of the laser-welded PWC-11 alloy.
2. Micro-hardness value of the FZ is increased primarily due to high cooling rate or solidification rate followed by dissolution of carbide precipitates owing to intense heat caused by the laser. Phase evolution and formation of niobium-based carbides, oxides and nitrides, which are hard and brittle in nature, contribute for the enhancement of micro-hardness.
3. Strength and ductility value of the FZ experiences a declination as compared to that of base metal. Lowering of yield point is caused due to dissolution of carbides, which is primarily added to arrest the dislocation movement during the deformation by the phenomenon of precipitation hardening alloy. Loss of ductility in the welded joints is mainly caused by the refined grains and improved hardness of FZ.

4. Analysis of the fractured surface of the uniaxial tensile test specimens presents mainly two types of failures, i.e., brittle and ductile failure. Brittle mode of failure occurs in the FZ, whereas the ductile mode of failure is found to be located in the base metal.

#### Acknowledgment

The authors gratefully acknowledge the funding of (Ministry of Human Resources Department) MHRD, Government of India, to carry out this study. The authors also like to thank Prof. Debalay Chakraborti of Materials and Metallurgical Department of IIT Kharagpur, India, for his technical insight and help for the work.

#### References

1. F. Heisterkamp, T. Carneiro, Niobium: Future Possibilities-Technology and the Market, *The International Symposium.*, 2001
2. B.P. Bewlay, M.R. Jackson, J.C. Zhao and P.R. Subramanian, A Review of Very High-Temperature Nb-Silicide-Based Composites, *Metall. Mater. Trans. A.*, 2003, **34**, p 2043–2052.

3. A. Hajitabar and H.N. Moosavy, Effect of Electron Beam Welding Current Variations on the Microstructure and Mechanical Properties of Nb-1Zr Advanced Alloy, *Vacuum*, 2018, **150**, p 196–202.
4. A. Sarkar, R. Kapoor, A. Verma, J.K. Chakravarty and A.K. Suri, Hot Deformation Behavior of Nb-1Zr-0.1C Alloy in the Temperature Range 700–1700°C, *J. Nucl. Mater.*, 2012, **422**, p 1–7.
5. B. Vishwanadh, S.K. Jha, K.V. Mirji, I. Samajdar, D. Srivastava, R. Tewari, N. Saibaba and G.K. Dey, Development of Nb-1%Zr-0.1%C Alloy as Structural Components for High Temperature Reactors, *J. Nucl. Mater.*, 2012, **427**, p 350–358.
6. B.P. Badgajar, S. Kumar, M.N. Jha, I. Samajdar, M. Mascarenhas, R. Tewari and G.K. Dey, An Investigation of Electron Beam Welding of Nb-1Zr-0.1C Alloy: Process Parameters and Microstructural Analysis, *J. Manuf. Process.*, 2017, **28**, p 326–335.
7. C. Silva, K. Leonard, M. Trammel and C. Bryan, Characterization of Different Forms of Zr-2.5Nb Samples Before and After Neutron Irradiation, *Mater. Sci. Eng. A.*, 2018, **716**, p 296–307.
8. B. O'Brien, Niobium Biomaterials, *Adv. Met. Biomater.*, 2015, **3**, p 245–272.
9. A. Chaudhuri, A. Sarkar, R. Kapoor, R.N. Singh, J.K. Chakravarty and S. Suwas, Microstructural Features of Hot Deformed Nb-1Zr-0.1C Alloy, *J. Miner. Metals Mater. Soc.*, 2014, **66**, p 1923–1929.
10. J. Maldonado, M. Kangelaski and P.J. Ring, PWC-11 Fabrication Methods for Optimum Strength for SP-100 Applications, *AIP Conf. Proc.*, 1994, **301**, p 1347–1352.
11. A.R.D. Costa, A. Craievich and R. Vilar, Niobium and Chromium Rich Coatings Tailored by Laser Alloying: XRD Analysis at High Temperatures, *Mater. Res.*, 2004, **7**, p 49–52.
12. I.V. Dulera, A. Basak, P.P. Kelkar and R.K. Sinha, Compact High Temperature Reactor (CHTR), *BARC Newslett.*, 2006, **273**, p 172–179.
13. R.H. Titran, T.J. Moore and T.L. Grobstein, Creep Properties of PWC-11 Base Metal and Weldments as Affected by Heat Treatment, *NASA Tech. Memo.*, 1986, **88842**, p 1–8.
14. D. P. Kramer, J. R. McDougal, B. A. Booher, J. D. Ruhkamp, E. I. Howell, Electron Beam and Nd-YAG laser welding of Niobium-1%Zirconium and Molybdenum-44.5% Rhenium thin sheet material, *35<sup>th</sup> Intersociety Energy Conversion Engineering Conference and Exhibit.*, 2000, **2971**, p 956–961
15. R. Smith, The Development of Oxidation-Resistant Niobium Alloys, *J. Less-Common Metals.*, 1960, **2**, p 191–206.
16. F. Franchini and P. Pierantozzi, Electron Beam Welding of Dissimilar Materials Niobium-Base Alloy C-103 with Titanium-Base Alloy Ti-6Al-4V ELI, *Weld. Int.*, 2009, **6**, p 792–797.
17. H. Hirose, K. Sato and T. Hayashi, Welding of Tantalum and Niobium, *Weld. Int.*, 2010, **8**, p 672–677.
18. M.H. Scott and P.M. Knowlson, The Welding and Brazing of the Refractory Metals Niobium, Tantalum, Molybdenum and Tungsten- A Review, *J. Less-Common Metals.*, 1963, **5**, p 205–244.
19. J. L. Kirchgessner, Forming and welding of niobium for superconducting cavities, *Proceedings of the Workshop on RF Superconductivity.*, 1984, p 533–543
20. R.G. Donnelly and G.M. Slaughter, Weldability Evaluation of Advanced Refractory Alloys, *Weld. J.*, 1966, **45**, p 250–257.
21. J.M. Gerken and J.M. Faulkner, Welding Characteristics of Advanced Columbium Alloys, *Weld. J.*, 1963, **45**, p 210–226.
22. M. Santella, J. McNabb and A. Frederick, Mechanical Properties of Nb-1Zr Weldments, *AIP Conf. Proc.*, 2005, **746**, p 845–853.
23. D.L. Olson, B. Mishra and D.W. Wenman, Welding, Brazing and Joining of Refractory Metals and Alloys, *Miner. Process. Extr. Metall. Rev.*, 2001, **22**, p 1–23.
24. S. Lampman, Weld integrity and performance *ASM International.*, 1997, p 6–10
25. T.K. Saha and A.K. Ray, Vacuum - the Ideal Environment for Welding of Reactive Materials, *J. Phys.: Conf. Ser.*, 2008, **114**, p 1–8.
26. A. Sanderson, C.S. Punshon and J.D. Russell, Advanced Welding Processes for Fusion Reactor Fabrication, *Fusion Eng. Des.*, 2000, **49–50**, p 77–87.
27. V.A. Kumar, M.K. Karthikeyan, E.G. Vinayan, R.K. Gupta, P.R. Kumar and P.P. Sinha, Electron Beam Welding Studies on Nb-Hf-Ti Refractory Alloy, *Mater. Sci. Forum.*, 2012, **710**, p 608–613.
28. P. Vondrous, L. Kolarik and M. Kolarikova, Plasma Arc Welding of NiTi and 304 Steel, *Ann. Proc. DAAAM Int.*, 2012, **23**, p 1039–1042.
29. L. Wu, Y. Wang, Z. Yan, J. Zhang, F. Xiao and B. Liao, The Phase Stability and Mechanical Properties of Nb-C System: Using First-Principles Calculations and Nano-Indentation, *J. Alloy. Compd.*, 2013, **561**, p 220–227.
30. E.J. Delgrosso, C.E. Carlson and J.J. Kaminsky, Development of Niobium-Zirconium-Carbon Alloys, *J. Less-Common Metals.*, 1967, **12**, p 173–201.
31. S. Majumdar, J. Kishor, B. Paul, R.C. Hubli and J.K. Chakravarty, Isothermal Oxidation Behavior and Growth Kinetics of Silicide Coatings Formed on Nb-1Zr-0.1C Alloy, *Corros. Sci.*, 2015, **95**, p 100–109.
32. S. K. Gupta, S. Datta, S. Jaypuria, D. K. Pratihari, P. Saha, A Critical Study of Bead-on-Plate Laser Welding of Niobium Alloy PWC-11, *Advances in Materials and Manufacturing Engineering.*, 2020, 397–404
33. S. K. Gupta, S. Jaypuria, D. K. Pratihari, P. Saha, Study on mechanical and metallurgical properties of fiber laser welded Nb-1% Zr-0.1% C alloy, *Optics & Laser Technology.*, 2020, **127**, 106153
34. C.C. Wojcik, Processing, Properties and Applications of High-Temperature Niobium Alloys, *Mater. Res. Soc. Symp.*, 1994, **322**, p 519–530.
35. K.J. Bal, J.D. Majumdar and A.R. Choudhury, Study on Uni-Axial Tensile Strength Properties of Ytterbium Fiber laser Welded Hastelloy C-276 Sheet, *Opt. Laser Technol.*, 2018, **108**, p 392–403.
36. M.J. Torkamany, F.M. Ghaini and R. Poursalehi, Dissimilar Pulsed Nd:YAG Laser Welding of Pure Niobium to Ti-6Al-4V, *Mater. Des.*, 2014, **53**, p 915–920.
37. S. Jaypuria, J. Meher, P.K.C. Kanigalpula and D.K. Pratihari, Electron Beam Butt Welding of Cu-Cr-Zr Alloy Plates: Experimental Investigations, Studies on Metallurgical and Mechanical Properties, *Fusion Eng. Des.*, 2018, **137**, p 209–220.
38. S.K. Gupta and P.K. Pal, Analysis of Through Transmission Laser Welding of Nylon6 by Finite Element Simulation, *Manag. Prod. En. Rev.*, 2018, **9(9)**, p 56–69.
39. P.K.C. Kanigalpula, S. Jaypuria, D.K. Pratihari and M.N. Jha, Experimental Investigations, Input-Output Modeling, and Optimization of Spiking Phenomenon in Electron Beam Welding of ETP Copper Plates, *Measurement*, 2018, **129**, p 302–318.
40. Minitab Inc. User Manual of MINITAB Statistical Software. Release 15 State College PA 16801 USA, 2007 ([http:// www.minitab.com](http://www.minitab.com))

**Publisher's Note** Springer Nature remains neutral with regard to jurisdictional claims in published maps and institutional affiliations.